



This is a repository copy of *Simulation of cortico-cancellous bone structure by 3D printing of bilayer calcium phosphate-based scaffolds*.

White Rose Research Online URL for this paper:  
<http://eprints.whiterose.ac.uk/117006/>

Version: Accepted Version

---

**Article:**

Almela, T., Brook, I.M., Khoshroo, K. et al. (7 more authors) (2017) Simulation of cortico-cancellous bone structure by 3D printing of bilayer calcium phosphate-based scaffolds. *Bioprinting*, 6. pp. 1-7. ISSN 2405-8866

<https://doi.org/10.1016/j.bprint.2017.04.001>

---

Article available under the terms of the CC-BY-NC-ND licence  
(<https://creativecommons.org/licenses/by-nc-nd/4.0/>)

**Reuse**

This article is distributed under the terms of the Creative Commons Attribution-NonCommercial-NoDerivs (CC BY-NC-ND) licence. This licence only allows you to download this work and share it with others as long as you credit the authors, but you can't change the article in any way or use it commercially. More information and the full terms of the licence here: <https://creativecommons.org/licenses/>

**Takedown**

If you consider content in White Rose Research Online to be in breach of UK law, please notify us by emailing [eprints@whiterose.ac.uk](mailto:eprints@whiterose.ac.uk) including the URL of the record and the reason for the withdrawal request.

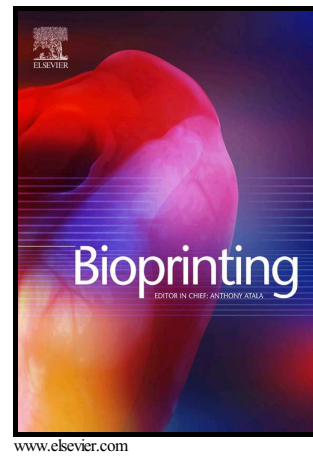


[eprints@whiterose.ac.uk](mailto:eprints@whiterose.ac.uk)  
<https://eprints.whiterose.ac.uk/>

## Author's Accepted Manuscript

Simulation of cortico-cancellous bone structure by 3D printing of bilayer calcium phosphate-based scaffolds

Thafar Almela, Ian M Brook, Kimia Khoshroo, Morteza Rasoulianboroujeni, Farahnaz Fahimipour, Mohammadreza Tahriri, Erfan Dashtimoghadam, Abdurahman El-Awa, Lobat Tayebi, Keyvan Moharamzadeh



PII: S2405-8866(16)30017-3  
DOI: <http://dx.doi.org/10.1016/j.bprint.2017.04.001>  
Reference: BPRINT8

To appear in: *Bioprinting*

Received date: 29 November 2016  
Revised date: 4 March 2017  
Accepted date: 11 April 2017

Cite this article as: Thafar Almela, Ian M Brook, Kimia Khoshroo, Morteza Rasoulianboroujeni, Farahnaz Fahimipour, Mohammadreza Tahriri, Erfan Dashtimoghadam, Abdurahman El-Awa, Lobat Tayebi and Keyvan Moharamzadeh, Simulation of cortico-cancellous bone structure by 3D printing of bilayer calcium phosphate-based scaffolds, *Bioprinting* <http://dx.doi.org/10.1016/j.bprint.2017.04.001>

This is a PDF file of an unedited manuscript that has been accepted for publication. As a service to our customers we are providing this early version of the manuscript. The manuscript will undergo copyediting, typesetting, and review of the resulting galley proof before it is published in its final citable form. Please note that during the production process errors may be discovered which could affect the content, and all legal disclaimers that apply to the journal pertain.

**Simulation of cortico-cancellous bone structure by 3D printing of bilayer calcium phosphate-based scaffolds**

Thafar Almela<sup>\*1</sup>, Ian M Brook<sup>1</sup>, Kimia Khoshroo<sup>2</sup>, Morteza Rasoulianboroujeni<sup>2</sup>, Farahnaz Fahimipour<sup>2</sup>, Mohammadreza Tahriri<sup>2</sup>, Erfan Dashtimoghadam<sup>2</sup>, Abdurahman El-Awa<sup>1</sup>, Lobat Tayebi<sup>2,3,4</sup>, Keyvan Moharamzadeh<sup>1,2</sup>

<sup>1</sup> School of Clinical Dentistry, University of Sheffield, Claremont Crescent, Sheffield, S10 2TA UK

<sup>2</sup> Department of Developmental Sciences, Marquette University School of Dentistry, Milwaukee, WI 53233, USA

<sup>3</sup> Biomaterials and Advanced Drug Delivery Laboratory, School of Medicine, Stanford University, Palo Alto, CA, USA

<sup>4</sup> Department of Engineering Science, University of Oxford, Oxford, OX1 3PJ, UK

\*Corresponding author: Tkalmela1@sheffield.ac.uk

### **Abstract**

Traditional methods of fabrication for porous bone scaffolds are unable to accurately mimic the desirable cortico-cancellous morphology and the structure of the bone. In this study, 3D printing of a  $\beta$ -Tricalcium phosphate (TCP)-based paste was used to develop scaffolds simulating the two distinct cortical and cancellous layers of the natural bone. Laser microscope imaging showed that the pore sizes were  $242.2 \pm 24.3 \mu\text{m}$  and  $410.5 \pm 27.9 \mu\text{m}$  for the cortical and cancellous layers, respectively. Micro CT analysis revealed overall porosity and interconnectivity of  $61.8 \pm 1.4\%$  and  $208707.5 \pm 52405$ , respectively. Mechanical properties were within the range of human cancellous bone with  $10.0 \pm 2.4 \text{ MPa}$  strength and  $55.5 \pm 5.7 \text{ MPa}$  young's modulus. The X-ray diffraction (XRD) analysis showed that the phase composition of the printed scaffolds was almost identical to pure TCP. Scanning electron microscopy (SEM) and cell vitality assessment indicated significant osteoblastic proliferation on the surface of the scaffolds. The gene expression analysis showed an increase in the level of Collagen I (Col I), Osteonectin (ON), Ostocalcin (OC), and

Osteopontin (OPN) with a significant increase in OC and OPN at day 10. In conclusion, 3D printing can be used to develop a TCP-based scaffold with controllable and reproducible microstructures and favourable in vitro biological properties with potential to be further developed to be used for clinical bone regeneration.

**Keywords:** 3D printing, scaffold, bone engineering, calcium phosphate, compact and cancellous bone

Accepted manuscript

## 1. Introduction

Bone grafts are often required to repair maxillofacial defects following trauma, cancer or developmental conditions such as cleft palate. However, the limitations associated with the use of autologous bone grafts or animal-derived products make the use of synthetic scaffolds an attractive alternative [1]. Fabrication of an ideal bone scaffold is an on-going medical challenge due to the complex hierarchical structure of the bone.

Scaffolds for osteogenesis should mimic the bone morphology, structure and function in order to optimize integration into the surrounding tissues. Bone is composed of hydroxyapatite  $\text{Ca}_{10}(\text{PO}_4)_6(\text{OH})_2$  crystals deposited within an organic matrix (95% type I collagen) [2]. Histologically, bone has inner trabecular layer which creates a porous environment with 50–90% porosity [3] and an outer cortical layer with 3–12% porosity. These two layers vary in their characteristics in terms of porosity, interconnectivity, pore size, mechanical properties, and surface area [2, 4].

Ideally, the scaffold should be made of appropriate biomaterial (s) to mimic the physical and chemical structure of the host tissue [5]. Calcium phosphates have been the primary focus for synthetic bone substitutes because of their osteoconductivity, biocompatibility, bioresorbability and chemical similarity to the inorganic phase of the bone [6]. The factors that govern the scaffold design are complex and include considerations of matrix architecture, pore size, morphology, mechanics versus porosity, surface topography and degradation products [7]. Conventional scaffold manufacturing methods such as particulate leaching [8], freeze-drying [9], and foam replication [10] have been used extensively.

Although high porosity can be achieved by these methods, the internal structure of the scaffold is difficult to control. Random and disconnected pores significantly decrease nutrient transportation, cell migration, and cell survival, especially in the centre of a bulky scaffold.

Recently, advances in computational design and additive manufacturing (AM) have enabled quick and accurate fabrication of 3D porous scaffolds with well-controlled architectures [11]. 3D printing is an alternative to current fabrication methods, facilitating precise production of 3D scaffolds with defined shape, size, porosity and pore size distribution which can have a significant impact on cell proliferation, differentiation, and vascularization [12-15]. In addition, it enables the use of various materials including polymers, ceramics, or composites. 3D printing thus has the capacity to produce the complex matrix structures that are not possible to be produced using conventional methods and thereby provided an optimal cell microenvironment with the potential to form functional tissue [7]. A limited number of studies have used different printing methods to fabricate TCP-based bone scaffolds with or without a binder [16]. These studies have produced scaffolds with single homogenous structure which do not simulate the bilayer cortico-cancellous structure of bone in most parts of the body and in the maxillofacial region.

The aim of this study was to exploit the advantage of 3D printing to fabricate a bilayer TCP-based scaffold that replicates the cortico-cancellous alveolar bone architecture.

## **2. Materials and Methods**

### **2.1 Fabrication of $\beta$ -TCP scaffold**

#### **2.1.1 Preparation of the printable $\beta$ -TCP paste**

An injectable TCP paste was formulated by mixing 1g Sodium Tripolyphosphate (TPP) (Alfa Aesar, US), 0.15g Carboxymethylcellulose Sodium salt (CMC) (Alfa Aesar, US), and 30g  $\beta$ -TCP powder (Sigma, US) in 10 ml deionized, filtered water. The paste was mixed and defoamed for 10 and 3 minutes, respectively at 2000 rpm using a centrifugal mixer (THINKY, Japan) and loaded into the plotting cartridge (Nordson, USA).

#### **2.1.2. 3D plotting of $\beta$ -TCP scaffolds**

The scaffolds were fabricated using the 3D bio plotting system (EnvisionTEC, Germany). By applying the optimized parameters as listed in Table 1, TCP paste was extruded from a cartridge through a plotting needle (Nordson, USA) having an inner diameter of 400 $\mu$ m. The printer head deposited strands of the paste in a layer-by-layer fashion on the building platform forming a disc of 10 mm x 2 mm thickness. Scaffolds were air-dried overnight and then sintered. Temperature of the furnace (Vulcan, USA) was raised to 600 °C at the uniform rate of 3°/min, held for 1 hour in 600, then raised from 600 °C to 1100 °C at a rate of 5°/min and remained at 1100 °C for 4 hours.

## **2.2 Characterization of scaffolds**

### **2.2.1 Structure, morphology, and surface topography**

Evaluation of the scaffold's morphology and surface roughness were conducted by 3D laser scanning digital microscope (Olympus LEXT OLS 4000, Japan). Scaffolds (n=6) were randomly selected to measure the roughness and dimension of the pores size, distance between strands, and thickness of strands in both sides of scaffolds using the software (LEXT OLS 4000).

### 2.2.2 Phase Composition

X-ray diffraction (XRD) was carried out for the scaffold powder and pure  $\beta$ -TCP from which the paste was prepared. Sintered scaffolds were ground using an agate mortar and pestle (Fisher scientific, UK). The powder was then sieved to 150  $\mu\text{m}$  particles (Endecotts, UK). XRD patterns were recorded between  $5^\circ$  and  $70^\circ$   $2\theta$  at a step of  $0.4^\circ/\text{s}$  using D<sub>2</sub> phaser diffractometer (Bruker, UK) equipped with a Cu K $\alpha$  radiation source of (30) KV and (10) mA. Diffraction data was analysed by ICDD PDF-4+ software (2015 edition).

### 2.2.3 Microstructural characterisation

The microstructural characteristics of the scaffolds (n=6) were quantitatively assessed by a high resolution micro-computed tomography  $\mu$ -CT scanner (SkyScan 1172; Bruker, Belgium) with a source voltage of 100 kV and current of 91  $\mu\text{A}$ . Specimens were mounted on a rotary stage and scanned at a rotation step of  $0.7^\circ$  over a total of  $180^\circ$ . All resulting 2D and 3D cross-sectional images were reconstructed and analysed using NRecon (version 1.6.10.4, Skyscan) and CTAn (version 1.13.2.1, Skyscan) softwares, respectively. Total, closed and open porosity, interconnectivity as well as the other basic features were determined.

### 2.2.3 Mechanical Properties

The young's modulus and ultimate compressive strength of the scaffolds were measured using a mechanical testing machine (Shimadzu, Japan) with a 5kN load cell, and a cross-head speed of  $1.0 \text{ mm min}^{-1}$ . The sintered cylindrical samples (n=5) with a diameter of 10 mm and a height of 20 mm were compressed in Z direction until they fractured. The data obtained was used to calculate the mean compressive strength and modulus.

### 2.2.4 Rheological Assessment

The rheological measurements were performed using a shear rheometer (Kinexus, Malvern, UK) with a stainless steel parallel-plate geometry with a diameter of 20 mm. The paste was placed on the lower plate and the upper plate was lowered until it gently touched the surface of the sample at a gap distance of 0.5 mm and excess material was removed. Measurements

were performed at different temperatures from 30 °C to 15 °C with a scanning interval of 5 °C. At each temperature, the rheological evaluation consisted of two consecutive shear cycles with no rotational pre-shear step. The shear rate varied linearly in ramp mode from 0 to 100 s<sup>-1</sup> with 10 s<sup>-1</sup> intervals in 2 min and then back to 0 s<sup>-1</sup>. The total testing time was 12 min.

## **2.3 Cell cultivation on $\beta$ -TCP scaffolds**

### **2.3.1. Cell isolation, culture and seeding**

The present study was conducted in accordance with the ethical approval granted by the Sheffield Research Ethics Committee (15/LO/0116, STH Research Department: STH18551). Human Osteoblasts (HOBs) were isolated from bone chips collected during dental implant surgery with the patients' written informed consent. HOBs were cultured in Dulbecco's modified Eagle medium (Gibco, UK) supplemented with 10%v/v fetal bovine serum, 100 U/ml penicillin and 100 mg/ml streptomycin, 625ng/ml Amphotericin B, and 50 $\mu$ g/ml Ascorbic acid (all supplements from Sigma, UK). Cells were incubated at 37 °C and 5% CO<sub>2</sub> and expanded up to the 3<sup>rd</sup> passage. The scaffolds were autoclaved and pre-incubated in the culture medium for 24 h, followed by cell seeding at a density of 2 $\times$ 10<sup>6</sup> per scaffold. The cell-scaffold constructs were cultured in spinner bioreactors for 10 days.

### **2.3.2 Cell viability and attachment**

Presoblu (PB) cell viability assay (Invitrogen, USA) was carried out according to the manufacturer's instructions after 1 and 10 days of tissue culture. The fluorescence (Ex: 560 nm and Em: 590 nm) were measured using a spectrophotometric plate reader (TECAN, USA). Scanning Electron Microscopy (SEM) was performed to observe the cell attachment and proliferation after 1 and 10 days. The scaffolds with and without the cells were removed from the culture medium, washed in PBS, fixed with 3% of glutaraldehyde, and dehydrated in gradient concentrations of 50, 60,70, 80, 90 and 100% ethanol. Samples were sputter-

coated with gold (~20 nm) and images were then captured at an acceleration voltage of 15 kV using a scanning electron microscope (Philips XL-20, USA).

### 2.3.3 Quantitative PCR (q-PCR)

Cell/scaffold constructs (n=5) were harvested for gene expression analysis at day 1 and 10 after incubation in the spinner bioreactor. RNA was isolated using isolate II RNA Mini Kit (BioLine) according to the manufacturer's instructions. The purity and concentration of the extracted RNA was measured with the NanoDrop 1000 Spectrophotometer (ThermoScientific) at 260/280 nm. Complementary DNA (cDNA) was synthesised in the thermal cycler (Bio-Rad Laboratories) using High Capacity RNA-to-cDNA Kit (Applied Biosystems, UK) in a 20 µl volume reaction, according to the manufacturer's instructions. The reverse transcription reaction consisted of 10 minutes at 25°C followed by 2 hours at 37 °C followed by 5 minutes at 85 °C, after which the sample was stored at 4°C. q-PCR was performed in triplicates using the Rotor-Gen Q (QIAGEN) in a 10 µl volume reaction containing 5 µl equal volumes of TaqMan universal PCR Master Mix, 0.5 µl B2M internal control (Applied Biosystems), 3.5 µl nuclease free water, and an equal volumes of cDNA and PCR primers for COL I (HS00164004), OCN (HS01587814), ON (HS00234160), and OPN (HS00959010). Cycling conditions were 95 °C for 10 seconds followed by 60 °C for 45 seconds and the cycle was repeated 40 times. The fluorescence was read at the end of the extension step and the data were analyzed using Rotor- Gen Q Software (QIAGEN). The expression level of the gene of HOBs was used as a positive control.

### 2.4 Statistical analysis

All the data were expressed as mean  $\pm$  standard deviation (Mean  $\pm$ SD). Statistical analysis was performed using GraphPad Prism 7.0 statistical analysis software. The significant difference was calculated by one-way and two-way ANOVA complemented by Tukey's and

Sidak's multiple comparisons tests. p values of  $<0.05$  and  $<0.0001$  were considered statistically significant.

Accepted manuscript

### 3. Results

#### 3.1 Morphology and surface roughness

The 3D laser microscopy examination revealed the differences between both sides of the 3D-printed scaffold in terms of pore size, strands thickness and distance between strands (Fig.1). For the compact side, the measurements showed  $242.2 \pm 24.3 \mu\text{m}$ ,  $516.8 \pm 28.1 \mu\text{m}$ , and  $214.5 \pm 19.1 \mu\text{m}$  respectively while the dimensions in the cancellous side were  $410.5 \pm 27.9 \mu\text{m}$ ,  $447.1 \pm 46.7 \mu\text{m}$ , and  $502.1 \pm 46.9 \mu\text{m}$ . The value of surface roughness (Ra) was  $1.1 \pm 0.2 \mu\text{m}$ .

#### 3.2 Phase Analysis

Fig. 2 shows the XRD patterns of the prepared  $\beta$ -TCP and crushed pure scaffold. As it can be seen in this figure, the crystalline structure of  $\beta$ -TCP was the major phase. Both the prepared scaffolds and pure  $\beta$ -TCP XRD patterns exhibited approximately the same characteristic peaks. No secondary phase, organic residue or crystallographic substitution were detected.

#### 3.3 $\mu$ CT-Scan

The basic properties of the scaffolds (n=6) determined by  $\mu$ -CT scanning are shown in the Table 2.

#### 3.4 Mechanical Properties

The compressive strength of the scaffolds was found to be  $10.0 \pm 2.4 \text{ MPa}$  while the modulus was  $55.5 \pm 5.7 \text{ MPa}$ . Both values are within the normal range of human cancellous bone (Young's moduli of 0.01–2 GPa, and the compressive strengths of 0.2–80 MPa).

### 3.5 Rheological Assessment

The viscosity assessment of the  $\beta$ -TCP paste indicates that the viscosity is strongly dependent on both shear rate and temperature. Fig. (3A) shows that at 15 °C the dependence of viscosity to shear rate is considerable for shear rate of 10 s<sup>-1</sup> to 70 s<sup>-1</sup>, while it remains constant at shear rates higher than 70 s<sup>-1</sup>. On the other hand, the effect of shear rate on viscosity is not significant when temperature is above 15 °C.

Regarding the temperature, Fig. (3B) shows that the decline in the viscosity started at 15 °C and ended at 20 °C. Increasing temperature up to 30 °C had no significant effect on the viscosity. The viscosity seems to be independent of the temperature for temperatures higher than 20 °C at a specific shear rate.

Fig.(3C) shows shear stress vs shear rate for the prepared paste at 20-30C. The paste seems to be a bingham plastic material with yield stresses of 58.12, 47.05 and 39.75 Pa at 20, 25 and 30C, respectively. A linear correlation between shear stress and shear rate was found for all the examined temperatures where all the coefficients of determination (R-squared) was found to be greater than 0.99.

The dependence of viscosity on temperature and shear rate influences the printing parameters i.e. cartridge temperature and printing pressure, respectively. The pressure applied on the material to print it dictates the material's flow rate from the needle which in turn could be related to the shear rate.

### 3.6 Cell morphology, viability and attachment

The reduction of Resazurin-based assay, (PB), is proportionate to the number of viable cells present in each scaffold. The results obtained from this assay are presented in Fig. 4 and show that the cell proliferation rate in day 10 is significantly higher than the cell proliferation rate in day 1 (P <0.05). This result is consistent with the qualitative SEM imaging which

revealed the macroporous interconnected scaffold structure that supported the cell adhesion, penetration, and growth on both surfaces of the scaffold during the 10-day culture period (Fig.5). In addition, the attached cells showed elongation and orientation along the scaffold strands which indicates that the osteoblasts spread and align along the surface microstructures.

### 3.7 Gene expression

The levels of osteoblastic gene expression for Col I, OC, OPN, and ON which were quantified by the real time PCR (RT-PCR) analysis, are illustrated in Fig. 6. On day 1, the expression of OPN was approximately 9 folds higher than that of the HOBs. Col I expression was two folds higher while OC and ON expressions were relatively similar to the HOBs. On day 10, the expression of all genes increased, however, OPN and OC were significantly higher than the expression level on day one with 29 folds and 6 folds increase for OPN and OC respectively ( $P < 0.0001$ ).

#### 4. Discussion

An important prerequisite for successful bone tissue engineering is utilization of a suitable scaffold that satisfies the physical and chemical requirements of the native bone. TCP is a well-established bone substitute material which has been used in combination with different techniques of scaffold fabrication such as leaching and foaming [17]. AM techniques enable more controlled construction of scaffold architecture and shape than using conventional scaffold fabrication methods [18]. In this study, we have described the use of 3D printing technology to fabricate TCP scaffolds with dual layers including compact and porous structures.

The flow rate of the dispensing material is a crucial aspect of 3D printing technique. This factor is known to affect the line width, fabrication time, and geometry resolution [19]. Our results indicate that the viscosity of the TCP paste is dependent on the shear rate and temperature to a certain extent. The prepared TCP paste, like many other ceramic slurries, has non-Newtonian behaviour and is a Bingham plastic material which means that the flow rate is directly proportionate to the shear stress and inversely to the viscosity (resistance to flow) [20, 21]. This feature can be advantageous in adjusting the viscosity of the dispensing paste by controlling the temperature, thereby, increasing the flow rate and shortening the fabrication time. However, the high dispensing speed may compromise the geometrical resolution.

The optimization of prepared paste and extrusion parameters allowed the fabrication of a TCP-based scaffold with certain characteristic features. Porosity and pores interconnectivity are two critical parameters that have a strong impact on the cell behaviour. Previous studies

have shown the optimum pore size for the bone is 400  $\mu\text{m}$  [22, 23], whereas the critical size is considered to be 100  $\mu\text{m}$  due to the cell size, migration and nutrition [24].

As human cancellous bone demonstrates a total porosity between 30% and 90%, a scaffold construct containing a porosity within this range is considered to be suitable for bone regeneration [3].

In the present study, it was possible to adjust the above parameters to be close to the optimized desirable values. In addition, the strand's thickness and the distance between the strands on the cancellous layers were tailored to be around or within the range of the trabecular struts in the cancellous bone which are approximately 100-300  $\mu\text{m}$  thick and have spaces equal to 300- 1500  $\mu\text{m}$  [25]. As the compact bone is denser than the cancellous bone, a higher resolution plotter is required to obtain a concentric rings similar to Haversian canals which are approximately 50  $\mu\text{m}$  in diameter [26].

With regard to the surface roughness, it is established that the surface topography can have positive effects on cellular functions because of unique properties such as increasing wettability and surface area. This can lead the cells to respond favourably in terms of protein secretion, adhesion, proliferation, and differentiation [27]. Wu et al.[28] investigated the influence of different degrees of roughness on the bone cells and they found that the optimum average roughness of 0.80~1.00  $\mu\text{m}$  could be a key factor in determining the morphological and functional cell responses. However, the cells exhibited a less activated proliferation when the surface roughness was above the critical point ( $R_a=1.00 \mu\text{m}$ ).

Although all the aforementioned factors are fundamentals for bone regeneration, a balance should be struck between these factors and maintaining proper mechanical properties. Mechanical strength is affected by the pore volume and distribution as well as the layer thickness and printing orientation [29]. These factors yield mechanical properties close to the

cancellous bone which ranged between 1.8-10.2 MPa and 10-2000 MPa for the compressive strength and modulus, respectively. These properties are lower than those of the compact bone which has a longitudinal compressive strength of 133-195 MPa and young's modulus of 11.7-18.2 GPa [25]. To counteract this problem, many methods have been used to reinforce the ceramic-based scaffolds including the infiltration of the bioactive glass with a tough Polycaprolactone (PCL) polymer [30], reinforcement with nano-titania particles [31], or compositing with collagen [32]. Recently, Roohani-Esfahani et al [33] have developed a 3D printed bioactive ceramic scaffold with a high compressive strength comparable to the compact bone (90-110 MPa at ~70% porosity). The authors attributed this result to the hexagonal pores architecture which resulted in higher contact area between the printed struts leading to an enhanced load transfer.

The last point to be considered is the cell-scaffold biological interaction which was evaluated by cell adhesion, proliferation, and gene expression. The osteoblasts alignment and spreading along the scaffold strands suggests that the newly produced bone matrix may exhibit anisotropic microstructure which in turn has its own impact on the mechanical properties [34]. In addition, the expression of collagen I, the major extracellular matrix protein, and the non-collagenous proteins, which are found in the bone and are known to be upregulated in the osteogenesis [35], indicate favourable in vitro biocompatibility of the printed scaffold and its ability to support bone tissue engineering.

## 5. Conclusion

This study disclosed the fabrication of a 3D-printed bilayer calcium phosphate cement-based scaffolds resembling the normal cortico-cancellous bone's microstructure. The scaffolds demonstrated optimal in vitro biocompatibility and biological activity, high interconnectivity, and precise pore size in both sides. The mechanical properties of the scaffolds were within the normal range of human cancellous bone. The 3D-printed bilayer bone scaffold developed in this study has the potential to be optimized and used as a suitable scaffold for bone tissue engineering and as a synthetic graft material in reconstruction of bony defects.

## 6. Acknowledgements

The authors are grateful to Caroline J Fry, Medical School, University of Sheffield, for help with the  $\mu$ -CT scan assessment.

## 7. Conflicts of Interest

The authors declare no conflict of interest.

## References

1. Kurien T, Pearson RG, Scammell B. Bone graft substitutes currently available in orthopaedic practice THE EVIDENCE FOR THEIR USE. *Bone Joint J*2013. p. 583-97.
2. Nanci A. Ten Cate's oral histology : development, structure, and function. 8th ed. / Antonio Nanci. ed. St. Louis, Mo.: St. Louis, Mo. : Elsevier, 2013.
3. Karageorgiou V, Kaplan D. Porosity of 3D biomaterial scaffolds and osteogenesis. *Biomaterials*. 2005;26:5474-91.
4. Cooper DM, Matyas JR, Katzenberg MA, Hallgrímsson B. Comparison of microcomputed tomographic and microradiographic measurements of cortical bone porosity. *Calcif Tissue Int*. 2004;74:437-47.
5. Chen QZ, Boccaccini AR, Zhang HB, Wang DZ, Edirisinghe MJ. Improved Mechanical Reliability of Bone Tissue Engineering ( Zirconia) Scaffolds by Electrospaying. *Journal of the American Ceramic Society*. 2006;89:1534-9.
6. Boccaccini AR, Ma PX, Boccaccini AR. Tissue engineering using ceramics and polymers. Second edition / edited by Aldo R. Boccaccini and Peter X. Ma. ed: Amsterdam : Elsevier, 2014.
7. Do AV, Khorsand B, Geary SM, Salem AK. 3D Printing of Scaffolds for Tissue Regeneration Applications. *Adv Healthc Mater*. 2015;4:1742-62.
8. Park H, Park C. Fabrication of 3d Porous Silk Scaffolds by Particulate (salt/sucrose) Leaching for Bone Tissue Reconstruction. *Tissue Engineering Part A*. 2015;21:S390-S.
9. Offeddu GS, Ashworth JC, Cameron RE, Oyen ML. Multi-scale mechanical response of freeze-dried collagen scaffolds for tissue engineering applications. *Journal of the Mechanical Behavior of Biomedical Materials*. 2015;42:19-25.
10. Baino F, Vitale-Brovarone C. Mechanical properties and reliability of glass– ceramic foam scaffolds for bone repair. *Materials Letters*. 2014;118:27-30.
11. Cox SC, Thornby JA, Gibbons GJ, Williams MA, Mallick KK. 3D printing of porous hydroxyapatite scaffolds intended for use in bone tissue engineering applications. *Mater Sci Eng C Mater Biol Appl*. 2015;47:237-47.
12. Wang MO, Vorwald CE, Dreher ML, Mott EJ, Cheng MH, Cinar A, et al. Evaluating 3D- Printed Biomaterials as Scaffolds for Vascularized Bone Tissue Engineering. *Advanced Materials*. 2015;27:138-44.

13. Shrivats AR, McDermott MC, Hollinger JO. Bone tissue engineering: state of the union. *Drug Discovery Today*. 2014;19:781-6.
14. Ferlin KM, Prendergast ME, Miller ML, Kaplan DS, Fisher JP. Influence of 3D printed porous architecture on mesenchymal stem cell enrichment and differentiation. *Acta Biomaterialia*. 2016;32:161-9.
15. Cavo M, Scaglione S. Scaffold microstructure effects on functional and mechanical performance: Integration of theoretical and experimental approaches for bone tissue engineering applications. *Mater Sci Eng C Mater Biol Appl*. 2016;68:872-9.
16. Bose S, Roy M, Bandyopadhyay A. Recent advances in bone tissue engineering scaffolds. *Trends in Biotechnology*. 2012.
17. Ginebra MP, Espanol M, Montufar EB, Perez RA, Mestres G. New processing approaches in calcium phosphate cements and their applications in regenerative medicine. *Acta Biomaterialia*. 2010;6:2863-73.
18. Lode A, Meissner K, Luo Y, Sonntag F, Glorius S, Nies B, et al. Fabrication of porous scaffolds by three-dimensional plotting of a pasty calcium phosphate bone cement under mild conditions. *J Tissue Eng Regen Med*. 2014;8:682-93.
19. Li MG, Tian XY, Chen XB. A brief review of dispensing-based rapid prototyping techniques in tissue scaffold fabrication: role of modeling on scaffold properties prediction. *Biofabrication*. 2009;1:032001.
20. Liu C, Shao H, Chen F, Zheng H. Rheological properties of concentrated aqueous injectable calcium phosphate cement slurry. *Biomaterials*. 2006;27:5003-13.
21. Qi X, Ye J, Wang Y. Improved injectability and in vitro degradation of a calcium phosphate cement containing poly(lactide-co-glycolide) microspheres. *Acta Biomaterialia*. 2008;4:1837-45.
22. Bai F, Wang Z, Lu J, Liu J, Chen G, Lv R, et al. The correlation between the internal structure and vascularization of controllable porous bioceramic materials in vivo: a quantitative study. *Tissue Eng Part A*. 2010;16:3791-803.
23. Feng B, Jinkang Z, Zhen W, Jianxi L, Jiang C, Jian L, et al. The effect of pore size on tissue ingrowth and neovascularization in porous bioceramics of controlled architecture in vivo. *Biomed Mater*. 2011;6:015007.
24. Rouwkema J, Rivron NC, van Blitterswijk CA. Vascularization in tissue engineering. *Trends Biotechnol*. 2008;26:434-41.

25. Bueno EM. Biologic foundations for skeletal tissue engineering. San Rafael, Calif.: San Rafael, Calif: Morgan & Claypool; 2011.
26. Burr DB, Allen MR. Preface. Basic and Applied Bone Biology. San Diego: Academic Press; 2014.
27. Zhao F, Wang J, Guo H, Liu S, He W. The Effects of Surface Properties of Nanostructured Bone Repair Materials on Their Performances. *Journal of Nanomaterials*. 2015.
28. Wu C, Chen M, Zheng T, Yang X. Effect of surface roughness on the initial response of MC3T3-E1 cells cultured on polished titanium alloy. *Biomed Mater Eng*. 2015;26 Suppl 1:S155-64.
29. Farzadi A, Solati-Hashjin M, Asadi-Eydivand M, Abu Osman NA. Effect of layer thickness and printing orientation on mechanical properties and dimensional accuracy of 3D printed porous samples for bone tissue engineering. *PLoS One*. 2014;9:e108252.
30. Eqtesadi S, Motealleh A, Pajares A, Guiberteau F, Miranda P. Improving mechanical properties of 13–93 bioactive glass robocast scaffold by poly (lactic acid) and poly ( $\epsilon$ -caprolactone) melt infiltration. *Journal of Non-Crystalline Solids*. 2016;432, Part A:111-9.
31. Feng P, Wei PP, Li P, Gao CD, Shuai CJ, Peng S. Calcium silicate ceramic scaffolds toughened with hydroxyapatite whiskers for bone tissue engineering. *Materials Characterization*. 2014;97:47-56.
32. Zhou CC, Ye XJ, Fan YJ, Qing FZ, Chen HJ, Zhang XD. Synthesis and characterization of CaP/Col composite scaffolds for load-bearing bone tissue engineering. *Composites Part B: Engineering*. 2014;62:242-8.
33. Roohani-Esfahani SI, Newman P, Zreiqat H. Design and Fabrication of 3D printed Scaffolds with a Mechanical Strength Comparable to Cortical Bone to Repair Large Bone Defects. *Sci Rep*. 2016;6:19468.
34. Nakano T., Matsugaki A., Ishimoto T., Todai M., Serizawa A., Suetoshi R., Fujitani W. Control of oriented extracellular matrix similar to anisotropic bone microstructure. *Materials Science Forum*, 2014; 783-786, 72-77.
35. Allori A., Sailon A., Warren S. Biological basis of bone formation, remodelling, and repair- Part II: Extracellular matrix. *Tissue Engineering, Part B: Reviews*, Vol.14(3), pp.275-284

**Tables and Figure captions**

**Fig. 1a** The 2D and 3D laser scanning images of the 3D-printed TCP scaffold showing the cancellous side (A and B), and the compact side (C and D).

**Fig. 1b** The pore dimensions in X and Y directions for the cortical part only that is not in contact with the platform.

**Fig. 2** The XRD analysis of TCP powders (pink) and the prepared scaffolds after sintering (blue).

**Fig. 3** The rheological assessment of TCP paste.

**Fig. 4** The PrestoBlue vitality assay.

**Fig. 5** Scanning electron micrographs of (A) and (B) acellular scaffolds, (C) and (D) osteoblast-seeded scaffold construct after 1 day of culture, and (E) and (F) cell-scaffold construct after 10 days of culture.

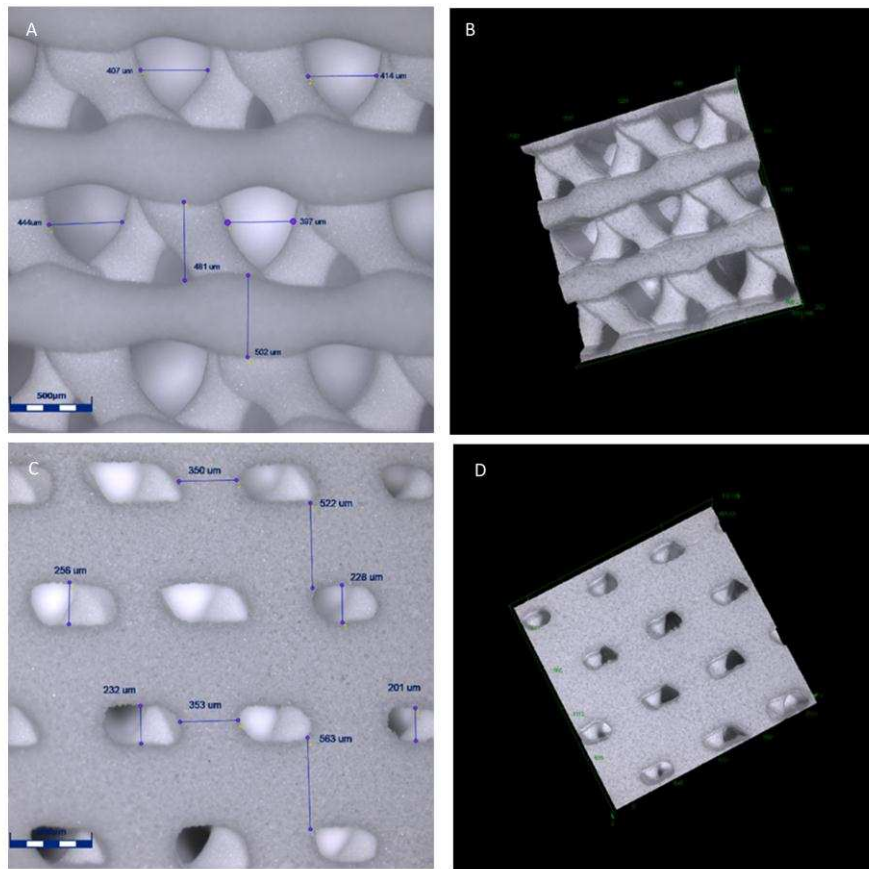
**Fig.6** Gen expression change of HOBs cultured on the printed scaffold for 10 days.

Table-1 The optimized parameters for printing the TCP

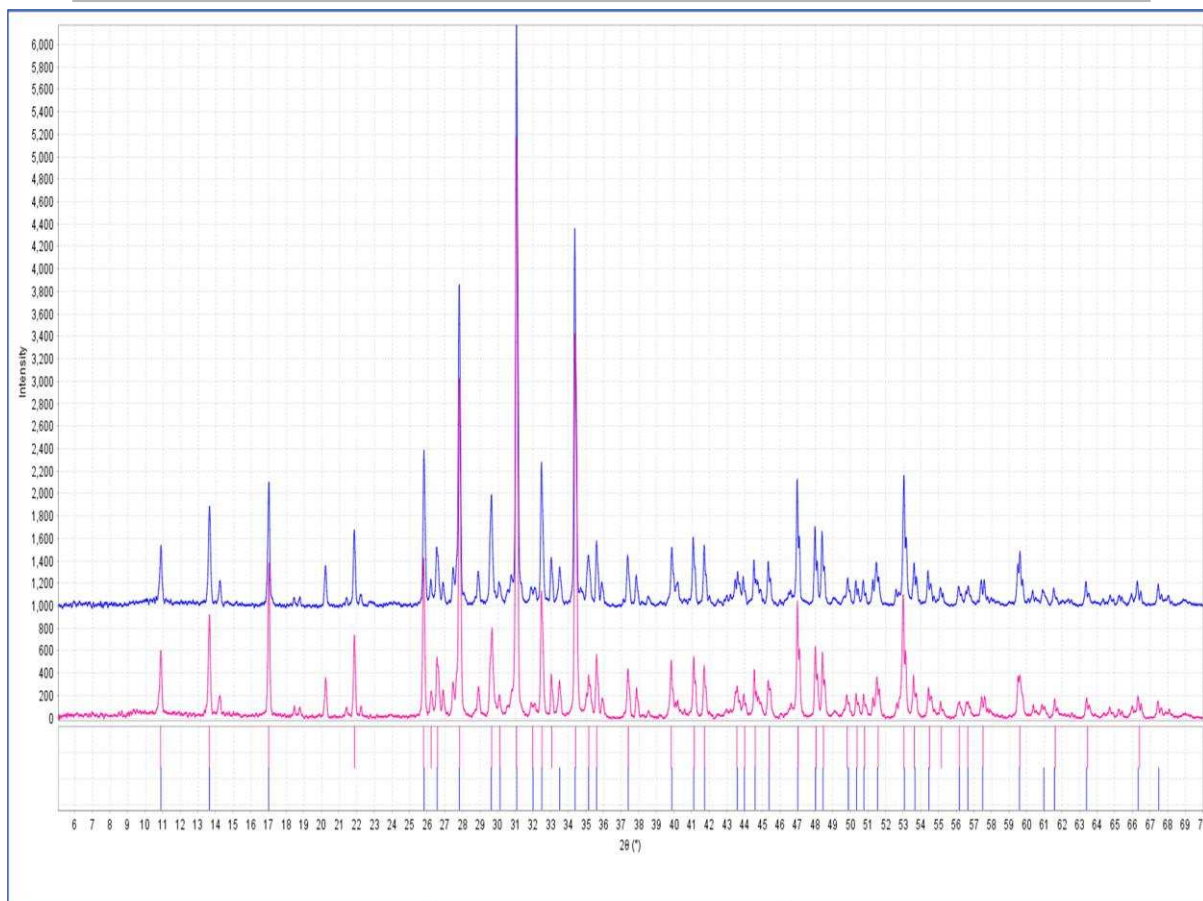
|   | <b>Parameter</b>         | <b>Measurement</b> |
|---|--------------------------|--------------------|
| 1 | Pressure                 | 1.5-1.7 bar        |
| 2 | Speed                    | 5 mm/s             |
| 3 | Material temperature     | 23 °C              |
| 4 | Platform temperature     | Room temperature   |
| 5 | Distance between strands | 0.6 mm and 0.8mm   |
| 6 | Lay down pattern         | 0°, 60°, 120°      |
| 7 | Slice width              | 150 $\mu$ m        |

Table-2 Micro-CT scanning measurements

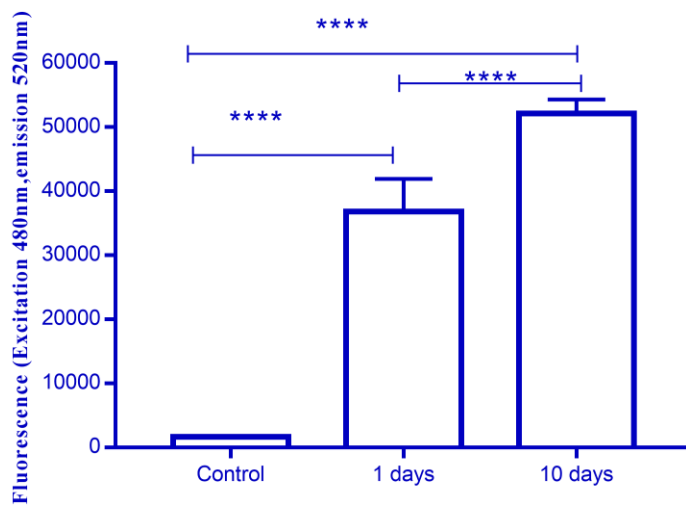
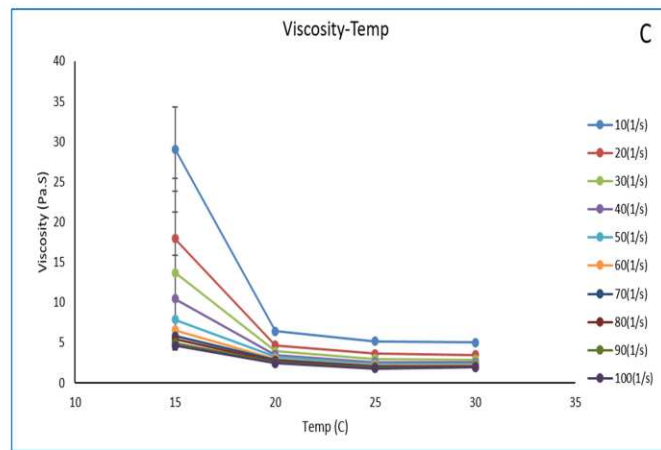
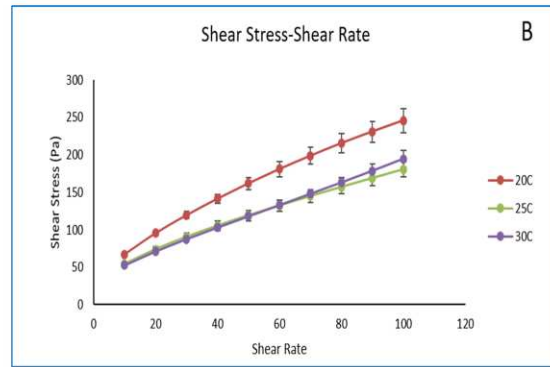
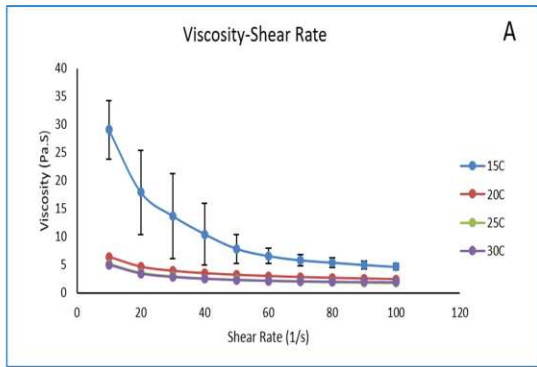
|   | <b>Feature</b>                             | <b>Mean <math>\pm</math> SD</b> |
|---|--------------------------------------------|---------------------------------|
| 1 | Closed porosity %                          | 0.040 $\pm$ 0.041               |
| 2 | Open porosity %                            | 61.8 $\pm$ 1.4                  |
| 3 | Total porosity %                           | 61.8 $\pm$ 1.4                  |
| 4 | Total volume of pore space mm <sup>3</sup> | 71.1 $\pm$ 1.6                  |
| 5 | Trabecular thickness mm                    | 0.05 $\pm$ 0.007                |
| 6 | Trabecular separation mm                   | 0.2 $\pm$ 0.02                  |
| 7 | Interconnectivity                          | 208707.5 $\pm$ 52405.1          |



Accepted manuscript

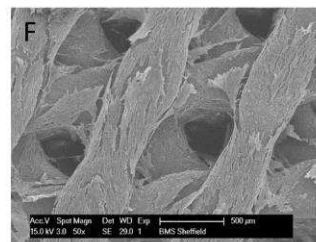
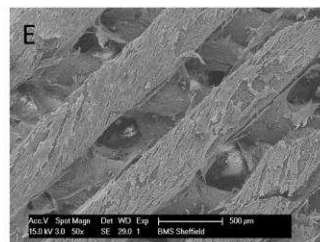
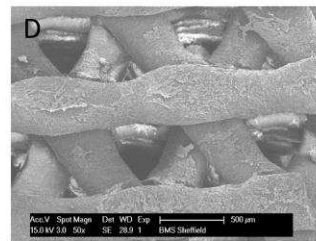
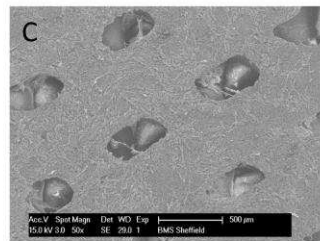
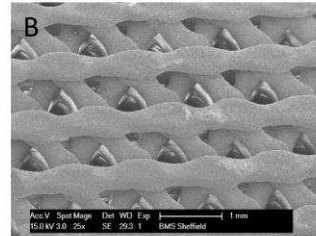
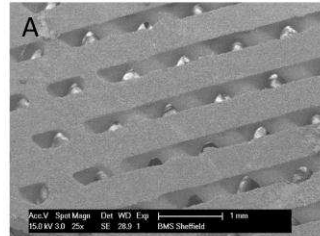


Accepted manuscript



Cortical layer

Cancellous layer



Accepted

